




DECEMBER 10, 2020

EVALUATING THE CARTOGRAPHIC QUALITY
OF ORTHOPHOTOS PRODUCED WITH A
REFINED PHOTOGRAMMETRIC POINT CLOUD

CAPSTONE PROJECT REPORT

MONICA CHISM
ADVISOR: PAT KENNELLY



Contents

Figures.....	3
Tables.....	3
Abstract.....	4
Introduction.....	4
Data Specifications.....	6
Project Area.....	6
Image Acquisition.....	6
Lidar Acquisition.....	6
Ground Control Collection.....	7
Methodology.....	8
Preprocessing.....	8
Phodar Testing and Processing.....	9
Post-Processing.....	14
Data Analysis.....	15
Discussion of Results.....	18
Phodar DEM vs Lidar DEM.....	18
Map Accuracy of Orthoimagery.....	18
Visual Quality of Orthoimagery.....	20
Conclusions.....	21
Conclusions for this Study.....	21
Considerations for Future Studies.....	22
Acknowledgements.....	23
Sources.....	24
Appendix.....	26

Figures

Figure 1. Aerial Imagery of the study area in Frankfort, Kentucky.	6
Figure 2. Data products used in this study.....	7
Figure 3. Overview of Processes Performed in the Study.....	8
Figure 4. Inpho Match-3DX Parameters with best resulting Phodar Surface for Bare-Earth Processing... ..	10
Figure 5. Relative Uniformity of the Lidar and Unfiltered Phodar Datasets.....	11
Figure 6. Relative Uniformity of the Lidar and Filtered Phodar Datasets.....	14
Figure 7. Inputs for Orthorectification.....	15
Figure 8. Example of Digitized Defects During the Visual QC Process.....	16
Figure 9. The Visual QC Process was Conducted via a Systematic Panning that Covered the Entire Project Area.....	16
Figure 10. NSSDA Horizontal Accuracy Computations (American Society for Photogrammetry and Remote Sensing, 2014; Federal Geographical Data Committee, 1998).	17
Figure 11. Comparison of the Relative Uniformity of the Phodar to the Lidar Before and After Filtering.	18
Figure 12. DEM-Derived Orthophoto Defects in Phodar and Lidar based Orthophotos.....	20

Tables

Table 1. TerraScan Macro Routine Parameters	12
Table 2. RMSE of Lidar-based and Phodar-based Orthophotos	19
Table 3. Lidar-Based Ortho GCP Test Results.....	19
Table 4. Phodar-Based Ortho GCP Test Results.....	19

Appendix

Appendix 1. Example of Smearred Orthoimagery Pixels	26
Appendix 2. Example of Smearing and Warping in Orthoimagery Pixels Encountered During Testing with Unfiltered Phodar	26
Appendix 3. Example of Bridge Warping in Orthoimagery	27
Appendix 4. Example of Building Warping.....	27

Evaluating the Cartographic Quality of Orthophotos Produced with a Refined Photogrammetric Point Cloud

Capstone Project Report by Monica Chism

Abstract

Orthorectified imagery can provide a detailed base for cartographic displays. This study investigates the accuracy and visual appeal of orthoimagery with the primary surface derived from phodar, a technique that uses photographic and orientation data. This research uses a stereoscopic image matching technology called Semi-Global Matching and Trimble's Inpho Match-3DX to generate a phodar surface. Orthoimagery resulting from refined phodar is compared to those generated with Lidar-based surface models. The results indicate accurate 3D placement of surfaces and associated orthoimagery, enhancing the cartographic quality of such imagery.

Introduction

Orthophotos are a crucial component for GIS data and mapping. They are used as a backdrop for digitizing GIS features and provides context for GIS data. Orthorectified aerial imagery is important for accurately representing distances on the ground. The process of rectifying aerial imagery corrects for geometric inaccuracies and terrain displacement created by elevated features in the image (Esri, 2019).

Among the most important elements of orthoimagery generation is the surface that is used during the orthorectification process (Hohle, 1996). When creating orthoimagery, an appropriate Digital Elevation Model (DEM) is not always available (Esri, 2019). Lidar datasets are the most widely used source of elevation data for the orthorectification process. As demand grows for high resolution orthoimagery with more rigorous accuracy specifications, the quality of the surface data has become more important.

The origin of surface data varies widely. Commonly used surface data for orthorectification include the National Elevation Dataset (NED), 3D Elevation Program (3DEP), Shuttle Radar Topography Mission (SRTM) data, manual stereo compilation and already existing or newly collected Light Detection and Ranging (lidar) data. Among these, the most recent lidar data is likely to be the most precise option outside of a manual compilation effort. SRTM and NED surfaces, which have some of the largest coverage areas, often cannot meet the accuracy requirements necessary for the current state of high-resolution aerial imagery.

Unfortunately, lidar data for a given project area may be unavailable, out of date, or variable in quality and processing technique. For example, at the time of this research in November of 2020, the 3DEP program, which is lidar covering all of North America (USGS, 2020), is likely to be the best available surface data for orthoimagery. The 3DEP dataset is incomplete and will include lidar spanning from 2016 to 2023 by its completion date in 2023. This can be problematic, because surface data that do not accurately represent the features as depicted in the aerial imagery do not make good surface models for orthoimagery production (Hohle, 1996; Švec & Pavelka, 2016). New lidar capture is expensive if existing data are not available (Blue Marble, 2018).

Regardless of the surface that is used for ortho production, even very precise surface data can be problematic when used to create orthorectified imagery. Examples of this dilemma (see Appendix 1-3) include skewing or warping of bridges, roads, or other man-made features and smearing of the imagery

where surface data might be too dense or missing (Švec & Pavelka, 2016). These DEM-related issues routinely appear when a surface model is applied to aerial imagery, but a quality bare-earth ground model helps to mitigate these issues in the final orthoimage by eliminating elevation spikes that cause such anomalies (Federal Geographic Data Committee, 1999).

This study investigates the use of photogrammetric point clouds (phodar) created for the production of orthoimagery. Phodar, like lidar, is a point cloud, but derived from pixel values in imagery. In this study, Match 3DX and TerraScan were used to automate the process of photogrammetric point cloud generation to create a bare-earth DEM that is suitable for creating accurate orthoimagery that is also as free of defects as can be achieved without manual editing.

Match 3DX is a recent addition to Trimble's Inpho photogrammetry software (Trimble, 2020). Match 3DX uses one of the newest algorithms developed for phodar creation called Semi Global Matching (SGM). Inpho can also perform an older method of image matching, Structure from Motion (SfM). SfM determines x, y, z-values based on overlapping images where objects must be present in all images. Because of this, the SfM process is more successful when there is more overlapping imagery (Widyaningrum & Gorte, 2017), which can result in the need for non-traditional aerial imagery flight plans so that there is sufficient imagery overlap. As such, SfM can be difficult to complete using imagery data that was not captured with the intended purpose being for use in SfM.

SGM can be more precise than previous phodar algorithms, generating a corresponding x, y, and z-value for most pixels in an image (Osińska-Skotak, Bakuła, Jełowicki, & Podkova, 2019). Using the SGM image matching technique, unlike SfM, neighboring values are taken into consideration when generating pixel coordinates, which creates a smoother appearance (Hirschmüller, 2008; Widyaningrum & Gorte, 2017) and the ability to rely less on image overlap. The SGM algorithm produces a denser point cloud than most lidar, making it suitable for the current needs of high-resolution aerial imagery (Gehrke, Morin, Downey, Boehrer, & Fuchs, 2010; Gehrke, Uebbing, Downey, & Morin, 2011). Additionally, it alleviates the need to rely on the cost of new lidar collection (Gehrke et al., 2010) or unreliable public data.

In 2011, Northwest Geomatics presented a SGM workflow for orthophoto production (Gehrke et al., 2011) that is compatible only with less common types of aerial imagery such as imagery that is collected with pushbroom sensors that is processed within the proprietary Leica XPro software package and not with the more traditional method of frame-based aerial photography. The details of that study, as well as training modules from Trimble and TerraScan software and collaboration with experts from Quantum Spatial Inc., a geospatial contractor, were considered when developing this workflow.

Goals and Objectives

The objective of this study is to evaluate if an SGM phodar surface is comparable in quality and accuracy to lidar when it is used in the production of high resolution orthophotos. An SGM phodar surface model was created in Inpho Match 3DX and was optimized for orthophoto production in an automated process. The phodar surface was assessed on its accuracy by comparing its differences from a QL2 lidar dataset, which is defined by the USGS in "Lidar Base Specifications" (United States Geological Survey, 2019). Additionally, map-accuracy and visual quality of orthophotos created from the phodar-derived DEM and lidar-derived DEM were compared.

Data Specifications

Project Area

The project area (Figure 1) to test the SGM approach is in Frankfort, Kentucky, USA. Frankfort is in the Inner Bluegrass region of Central Kentucky and the center of downtown is bisected by the Kentucky River, which is lined with limestone outcrops. This region is known for gently rolling hills and river valleys with an elevation ranging from about 400 to 950 ft AMSL (University of Kentucky, 2020). This project area was chosen in part because it encompasses various terrain features that are notorious for creating distortions and artifacts in orthophotos (Esri, 2019) and also because at the time of this study, the Commonwealth of Kentucky's Office of Technology Division of Geographic Information (Ky DGI) had recently acquired aerial lidar and imagery collected in the spring of 2019 that could be used for head to head testing.

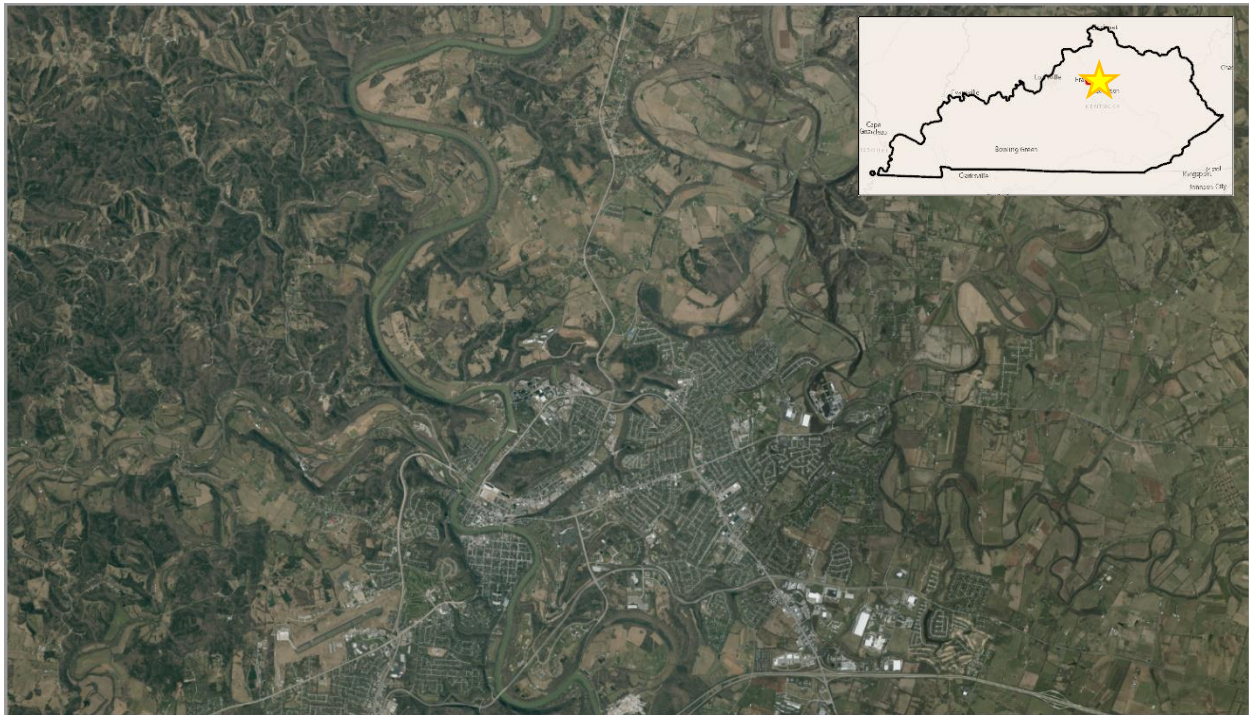


Figure 1. Aerial Imagery of the study area in Frankfort, Kentucky.

Image Acquisition

A 100 square mile subset of an approximately 20,000 square mile leaf-off imagery dataset (KYAPED, 2019a) that was captured for Ky DGI between February and April 2019 was used for the image processing, photogrammetric SGM surface processing, and orthorectification in this study. The dataset, which contained 8-bit, multi-spectral RGBN, 6-inch resolution imagery was captured by a Vexcel UltraCam Eagle Mark I approximately 9,300 feet above ground level, a suitable height to create a 0.5 foot per pixel ground sample distance (GSD) orthophoto. The imagery was acquired with a flight plan of 60 percent forward and 30 percent side (between flight line) overlap (Kentucky Division of Geographic Information, 2019).

Lidar Acquisition

The lidar used for this study is a 100 square mile subset of a QL2 Lidar Dataset (KYAPED, 2019c) for Ky DGI that covered approximately 6,630 square miles and was captured between February and March 2019. The

lidar point cloud was captured by a Leica ALS 80 approximately 7,550 feet above ground level with an average point density of 2 ppsm (points per square meter).

Ground Control Collection

A subset of ground control points (GCPs) that were collected between 2012 and 2019 (KYAPED, 2019b) for Ky DGI were used in this research. The imagery and lidar data that were retrieved from KYAPED for use in this study both used subsets of said ground control points for data processing. In the lidar, they were used for ground truthing, and in the imagery data, they were utilized as control in the aerotriangulation processing. In addition, six of these points fall only within the AOI used for this study and were used as a measure of accuracy on the orthoimagery. These six GCPs were recorded in NAD83 (2011) Kentucky State Plane Single Zone Geoid 12A.

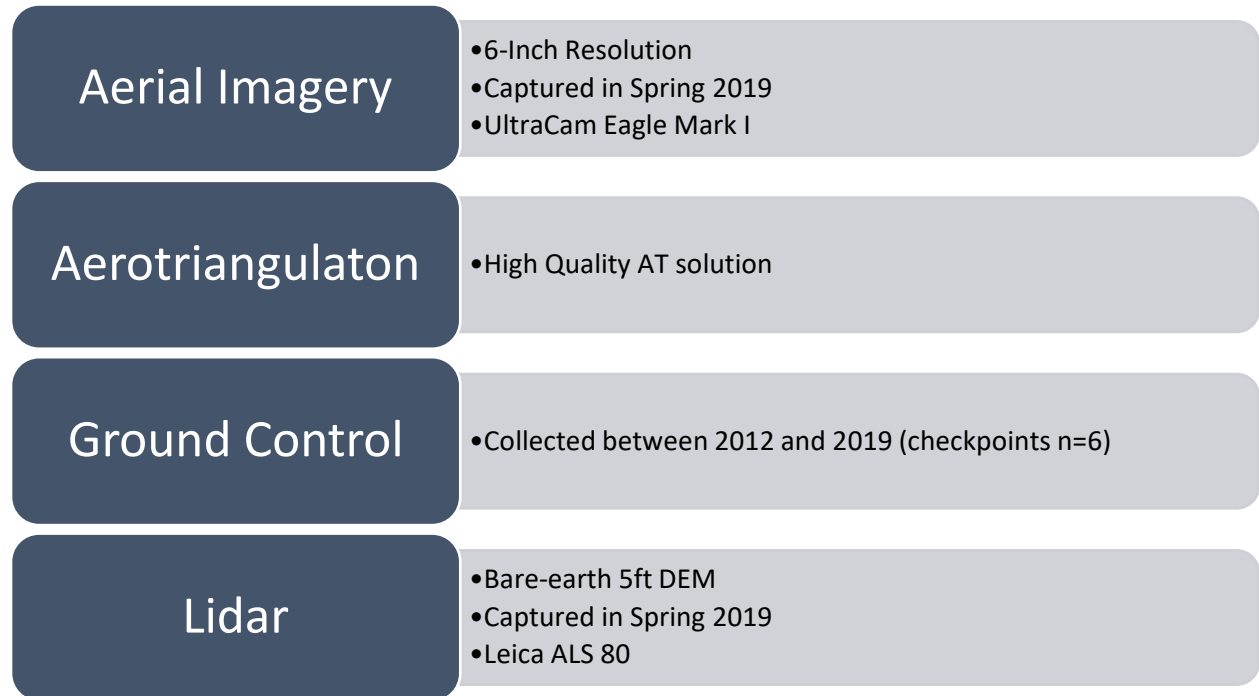


Figure 2. Data products used in this study

Methodology

This section explains the processing of the data that were used in this study, as well as the testing steps that were taken to identify the optimal parameters to create a phodar SGM point cloud that is suitable for orthorectification of aerial imagery. The discussion of these methods (see Figure 3) includes the preprocessing, testing, post-processing, and analyses of the resulting data that were performed to achieve the goals and objectives of this study.

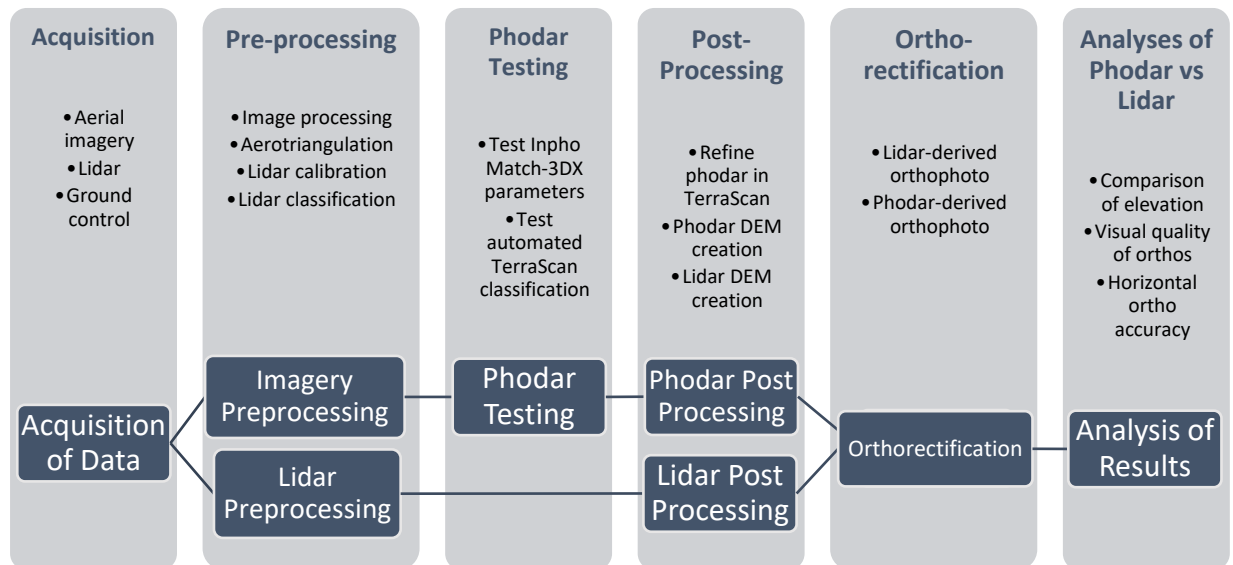


Figure 3. Overview of Processes Performed in the Study

Preprocessing

To support the objectives of this study, the lidar, imagery, and ground control were subjected to a preprocessing phase prior to the main processing phase. These processes were performed by geospatial contractor, Quantum Spatial, which acquired the data and processed it for Ky DGI. These steps are important to note in this study, so their parameters are discussed below, but a full review of these processes is not necessary because they are routine and not unique to these datasets.

Image Preprocessing

The imagery data were developed using Vexcel UltraMap software, which is supplemented by orientation, sensor, and airborne GPS and inertial measurement unit (ABGPS/IMU) datasets, which were captured simultaneously with the imagery to determine photo position and orientation. The ABGPS and IMU were processed with Applanix POSPac software. This processing environment uses several parameters, such as GPS variance, altitude, aircraft trajectory, and satellite information to gauge accuracy (Quantum Spatial, 2019b).

Aerotriangulation Preprocessing

“Image orientation is a prerequisite for generating DEMs and orthoimagery” (Esri, 2019). The process of aerotriangulation uses interior and exterior orientation information calculated during imagery processing along with supplemental ground control coordinates to position the captured aerial imagery in the correct

spatial position. With an approximate spatial position determined during imagery processing, aerotriangulation software can use imagery overlaps to generate automated points (tie points) that tie the imagery together based on similar pixels. The ground control coordinate locations are measured manually across tied images to ground the data to real world coordinates (Esri, 2019). This is a basic process of photogrammetry and no process was performed out of the ordinary in this dataset. Image Station Aero Triangulation software was used to perform aerotriangulation (Quantum Spatial, 2019b). This project was imported into Inpho Match-T software so that it could be used for the phodar processing in Inpho Match-3DX. This process was crucial to the accuracy of the phodar dataset.

Lidar Preprocessing

The lidar point clouds used in this study were generated using Leica CloudPro software and calibrated using TerraScan. Calibration readies the point cloud data for classification. The ABGPS and IMU data were processed with Inertial Explorer. This processing environment uses several parameters, including GPS variance, altitude, aircraft trajectory, and satellite information to gauge accuracy (Quantum Spatial, 2019a).

The point cloud was classified using manual and automated classification methods into industry standard classes, 1 through 20, utilizing digitized vector breaklines to classify waterbodies. Bare-earth, class 2, was isolated and processed into a 5-foot resolution Digital Earth Model (DEM) for use in this study.

Phodar Testing and Processing

Using the preprocessed imagery data, various models of differing parameters were tested with the Match-3DX software to determine optimal software parameters for the SGM phodar surface creation within the software. Each set of parameters tested was applied across the entire project area covering urban and forested areas and waterbodies to determine the parameters with the best results. The best resulting surface model was used to create orthoimagery that was tested for its accuracy according to National Standard for Spatial Data Accuracy (NSSDA) procedures (American Society for Photogrammetry and Remote Sensing, 2014; Federal Geographical Data Committee, 1998) to the greatest extent possible. The phodar DEM dataset was compared to the lidar DEM dataset and the variance between the two datasets were examined. The results are discussed in the data analysis section.

During the process of testing phodar surfaces created using different parameters, there were a range of issues that were present. The main types of errors resulted from missing data and points located in treetops. These are typical issues that are presented in phodar creation due to the processes' inability to penetrate through vegetation to capture the ground surface like lidar can. Additionally, there were missing, or erroneous z-values located within the water bodies. These issues are problematic when the point cloud is processed to create orthoimagery, resulting DEM-related distortions such as a smeared appearance or warped features. The processing parameters which showed the best results are shown in Figure 4. These parameters are SGM, unfiltered 3D point cloud, Digital Terrain Model (DTM) parameters within the 3DX processing interface.

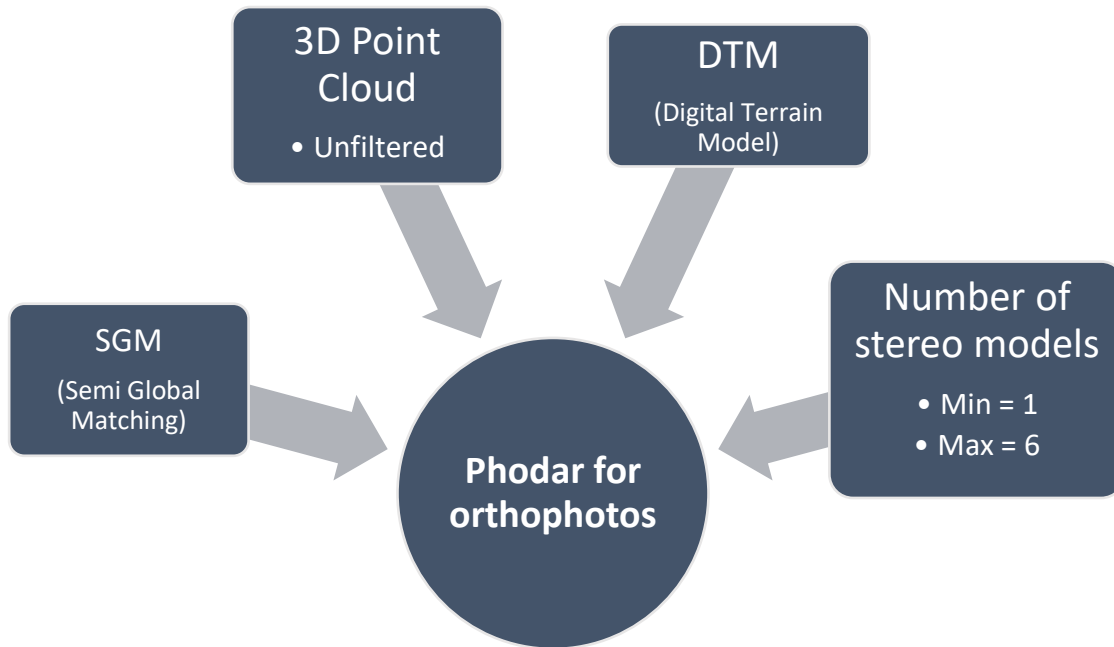


Figure 4. Inpho Match-3DX Parameters with best resulting Phodar Surface for Bare-Earth Processing

After the final phodar point cloud was processed using the parameters shown in Figure 4, a raster DEM was created for further evaluation. Because the phodar point cloud was processed as a DTM, it should have theoretically contained only bare-earth points. So, the phodar point cloud was processed with all points as a 5-foot pixel spacing DEM in the coordinate system of State Plane NAD83 Kentucky Single Zone in US Feet. When the guidelines of this study were developed it was expected that the phodar would likely contain more than bare-earth values.

In observing the phodar DEM, it was noted that, when compared to the bare-earth lidar DEM, the range of elevations in the phodar DEM was higher than in the lidar DEM. To illustrate this difference, the relative uniformity of the phodar and the lidar are shown in Figure 5. Because of the nature of phodar processing it was determined that the z values were likely to be vegetation and building elevations that made it into the DTM. To validate the hypothesis that these above-ground elevations would negatively affect the orthophoto, random samples were generated and as expected, they contained significant DEM-related distortions, such as smearing and warping (see Appendix 2).

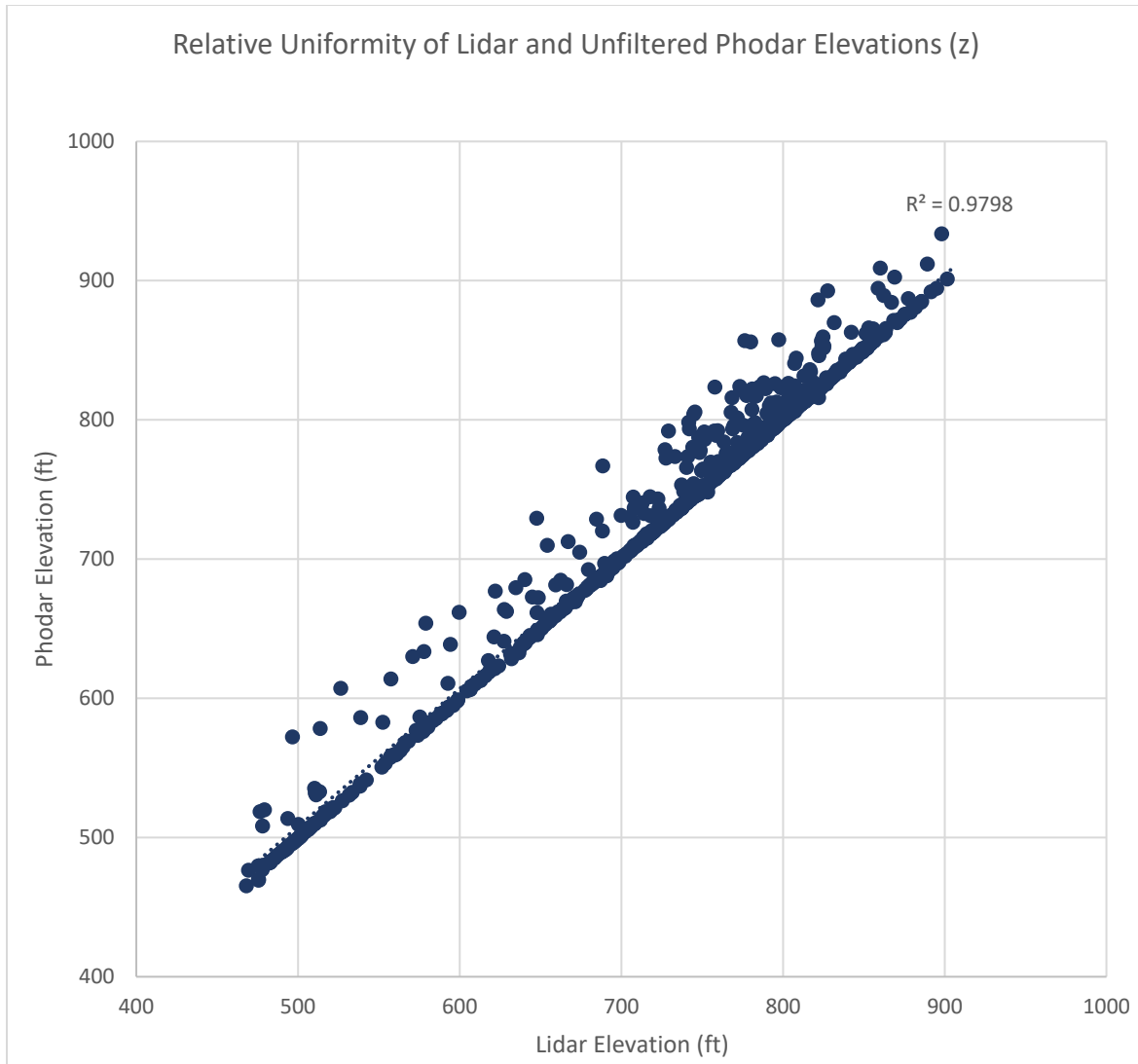


Figure 5. Relative Uniformity of the Lidar and Unfiltered Phodar Datasets

The remainder of the testing phase was dedicated to filtering and classifying the phodar surface to better reflect only bare-earth. This processing occurred in TerraScan software, which is a point cloud editing software that was used within Microstation Connect. The focus of this testing was to create an automated lidar classification that filtered the phodar point cloud into as close to a bare-earth model as possible.

In TerraScan, routines can be performed that consist of steps that are based on certain conditions. When the conditions are met, it can eliminate erroneous and poorly classified points in the point cloud. This routine was specifically focused on taking an unclassified phodar dataset and creating a class 2 (ground) bare-earth point cloud, eliminating high or low points, points located on top of vegetation, and points located on top of buildings. A general summary of the steps taken in this routine are shown in Table 1.

Table 1. TerraScan Macro Routine Parameters

	Step	Parameters	Details (based on this terrain in ft)
Preparation and Removal of Outliers to Define Ground	Classify by Class	Any Class to Unclassified	All points started as "never classified." Moves all points to "Unclassified" class.
	Classify Absolute Elevation	Any Class to Noise	Any point with extremely low elevation moves to "Noise" class (-9999 to -100).
	Classify Isolated Points	Unclassified within a specified distance to Noise	Any Unclassified points isolated within 6ft of another moves to Noise Class.
	Classify Hard Surface	Any Class to Model Key	Using "Model Key" as a temporary ground class, any points of median range elevation are moved to Model Key (MK).
	Classify Height Above Ground	Unclassified to Model Key	Moves any point still Unclassified and within +/-0.05 ft of a MK point to MK. Max triangulation distance of 250 ft. Adds more points that are suspected ground to the MK class.
	Classify Air	Model Key to Unclassified	Removes points from MK back into Unclassified if fewer than 5 points within a 50 ft radius.
	Classify Low (Group)	Model Key to Noise	Searches groups of 20 or less MK points within a 20 ft radius to find points that are >2 ft lower than other points and moves them to Noise.
	Classify Low (Single)	Model Key to Noise	Is run in multiple iterations to search for single points within a 20 ft radius to find points that are >2 ft lower than other points and moves them to Noise.
Define Ground Class	Classify Ground	Model Key to Ground	Moves MK points to Ground class. Uses Aerial Low (first ground classification) & 360 ft building length tolerance with an 88-degree terrain angle, 16-degree iteration, and a 3.5 ft iteration distance.
	Classify Ground	Model Key to Ground Current Ground only	Moves a second iteration of MK points to Ground class. Initial points are current ground only. Other parameters are the same as the previous except with a 1.4 ft iteration distance.

Refine Ground Class	Classify Below	Ground to Noise	Finds pits in the Ground class and moves them to Noise. Max allowed elevation variation (z tolerance) of 0.03 ft.
	Classify Low (Group)	Ground to Noise	Searches groups of 20 or less Ground points within a 60ft radius to find points that are >2 ft lower than other points and move them to Noise.
	Classify Low (Single)	Ground to Noise	Removes additional low points from Ground to Noise class using above parameters, but on single points.
	Classify Air	Ground to Unclassified	Removing points from Ground back into Unclassified if fewer than 5 points within a 100 ft radius.
	Classify Class	Model Key to Unclassified	Moves all remaining MK points not classified to ground back to Unclassified before a final clean up.
	Classify Height Above Ground	Unclassified to Ground	Moves any point in Unclassified and within +/-0.05 ft of a Ground point to Ground. Max triangulation distance of 50 ft. Anything within 0.05 ft at this point is likely to be ground.
	Classify Height Above Ground	Unclassified to Noise	Moves any point in Unclassified and within -9999 to -5 ft of Ground back to Noise. Max triangulation distance of 50 ft. Removing any remaining low outliers back to Noise.

After completing the macro routines on the phodar point cloud in TerraScan, the final LAS files were exported, compared to the lidar, and then used for orthorectification. These steps are detailed in the post-processing section.

Post-Processing

The post-processing phase for this study consisted of preparing the resulting phodar dataset into a product that can be used to do a head to head comparison with the lidar dataset. A phodar DEM with the same specifications as the lidar DEM was prepared. This DEM was used to create two sets of orthoimagery, using the phodar and lidar DEMs, respectively, for quality comparison.

To prepare the final filtered and classified phodar point cloud for orthorectification, it was processed into a 5-foot pixel spacing raster DEM in the coordinate system State Plane Kentucky Single Zone NAD 83 in US Feet. To visualize the difference that the filtering process made in the phodar elevations, another scatterplot showing its elevation values' relative uniformity to those of the lidar dataset is shown in Figure 6. It is apparent from the R^2 value and comparing Figure 6 to Figure 5 that the filtering made a significant improvement in the phodar dataset's uniformity to the lidar dataset. It is hypothesized that filtering the points in TerraScan will provide a phodar surface more closely resembling lidar bare-earth, making it a more accurate surface product and more suitable for creating an accurate orthophoto with minimal visual defects.

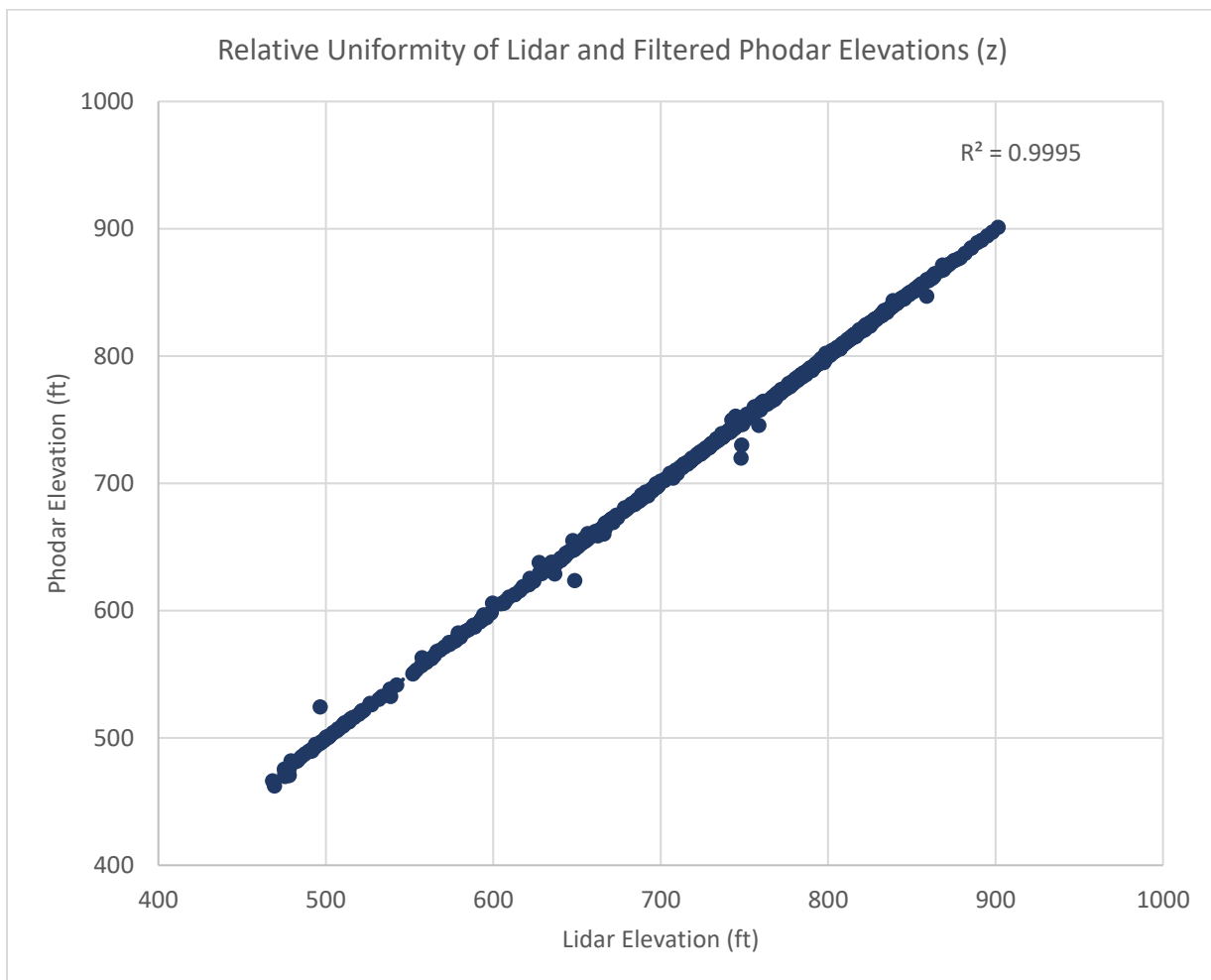


Figure 6. Relative Uniformity of the Lidar and Filtered Phodar Datasets

To test this theory, orthorectification using each surface was performed (Figure 7). Orthorectification utilizes the aerotriangulation and surface data to remove distortions associated with camera tilt and ground relief and create a uniform scale throughout the imagery (Esri, 2019). Image Station OrthoPro software was used to create two sets of orthophotos. Using the same aerotriangulation, images, and seamlines as input, a set of lidar-derived orthophotos and a set of phodar-derived orthophotos were processed with a 0.5-foot pixel resolution in the coordinate system of State Plane Kentucky Single Zone NAD 83 in US Feet and were clipped into a tiled grid format to create a manageable file size for evaluation.

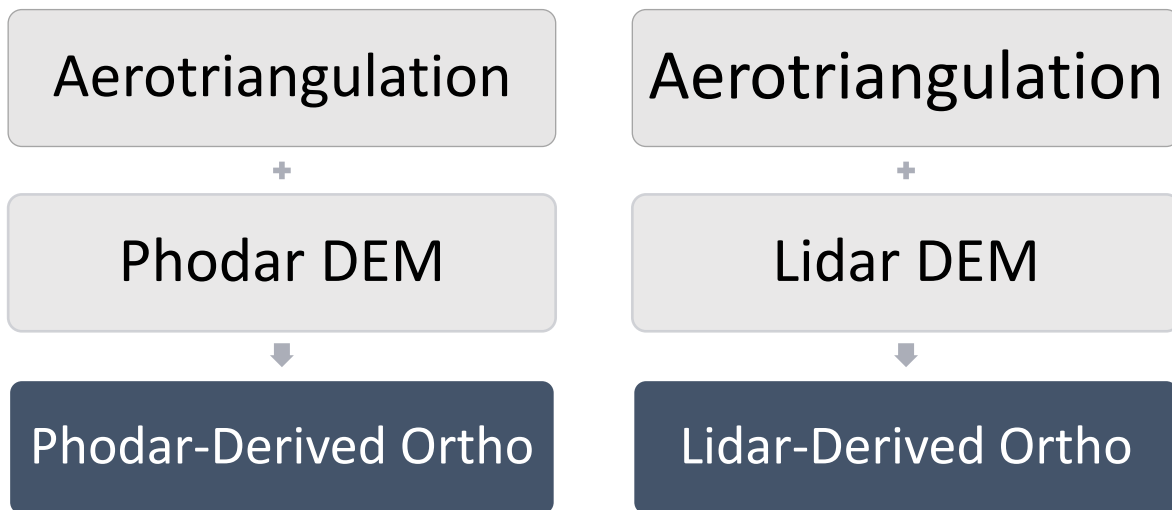


Figure 7. Inputs for Orthorectification

Data Analysis

To evaluate the orthorectified data, a series of quality control (QC) and accuracy analyses were performed.

The QC process was performed on both the lidar-derived and phodar-derived orthophotos to assess the visual quality and tabulate the number of DEM-related geometric distortions found within each set of orthoimagery (Figure 8). DEM-related defects that were accounted for in this QC are smeared features, warped bridges, and “other” warped features such as roads, buildings, or retaining walls. Each ortho dataset was subjected to a systematic visual inspection, performed at a consistent zoom level panning across the entire dataset (Figure 9), a process that is typical in orthoimagery production to determine the acceptability of an image (Federal Geographic Data Committee, 1999). The total number of defects detected in each dataset of orthophotos were digitized in vector format (Figure 8) for comparison.



Figure 8. Example of Digitized Defects During the Visual QC Process

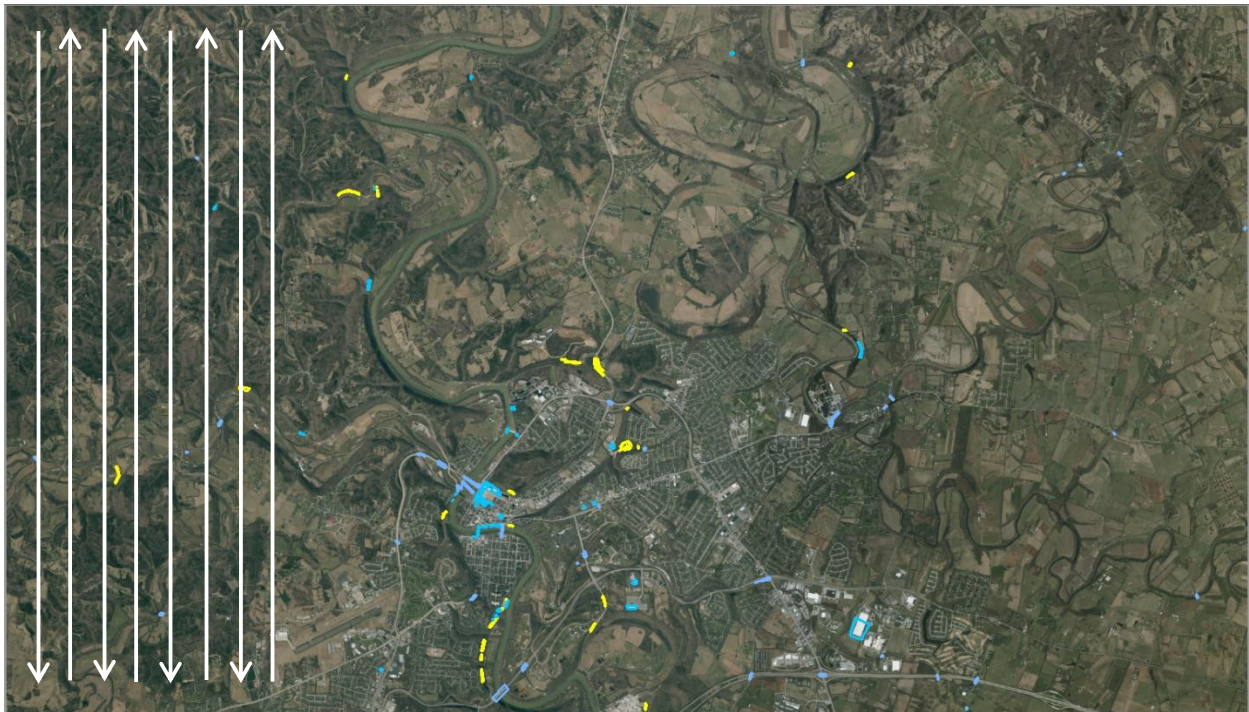


Figure 9. The Visual QC Process was Conducted via a Systematic Panning that Covered the Entire Project Area

To evaluate the accuracy of the lidar-derived and phodar-derived orthophotos, a series of six ground control points (GCP) were measured using Compass Data Accuracy Analyst software. This software allows the user to measure known X and Y values from GCPs against their location on the orthophotos and calculates the difference using NSSDA guidelines for calculating the Root Mean Square Error (RMSE)

(Figure 10). It should be noted that the NSSDA and ASPRS guidelines for positional accuracy recommend a minimum of 20 checkpoints for evaluation, but this project area encompassed only six GCPs, all of which were used for evaluation.

NSSDA Horizontal Accuracy Computations

$$\text{RMSE}_{\text{northing}} = \sqrt{\sum (\text{CONTROL}_{\text{northing}} - \text{MEASURED}_{\text{northing}})^2 / n}$$
$$\text{RMSE}_{\text{easting}} = \sqrt{\sum (\text{CONTROL}_{\text{easting}} - \text{MEASURED}_{\text{easting}})^2 / n}$$
$$\text{RMSE}_r = \sqrt{\text{RMSE}_{\text{easting}}^2 + \text{RMSE}_{\text{northing}}^2}$$

95 % Confidence Level Accuracy = 1.7308 * RMSE_r

Figure 10. NSSDA Horizontal Accuracy Computations (American Society for Photogrammetry and Remote Sensing, 2014; Federal Geographical Data Committee, 1998).

Discussion of Results

Three qualitative analyses were performed on the data resulting from this study: a comparison of the phodar DEM to the lidar DEM, a comparison of the accuracy of the phodar-derived orthoimagery to the lidar-derived orthoimagery, and also a comparison of the visual quality of the phodar-derived orthoimagery to the lidar-derived orthoimagery. The results are as follows.

Phodar DEM vs Lidar DEM

The relative uniformity of the phodar was compared to the lidar prior to and following the filtering of the phodar point cloud in TerraScan. The results are shown side by side in Figure 11. The data shows that lidar accounts for 99.95% of the variability of the refined phodar elevation points. To further confirm the necessity of bare-earth filtering of the phodar, sample orthos were generated and contained significant pixel smearing in areas that contained vegetation or noise points (see Appendix 2).

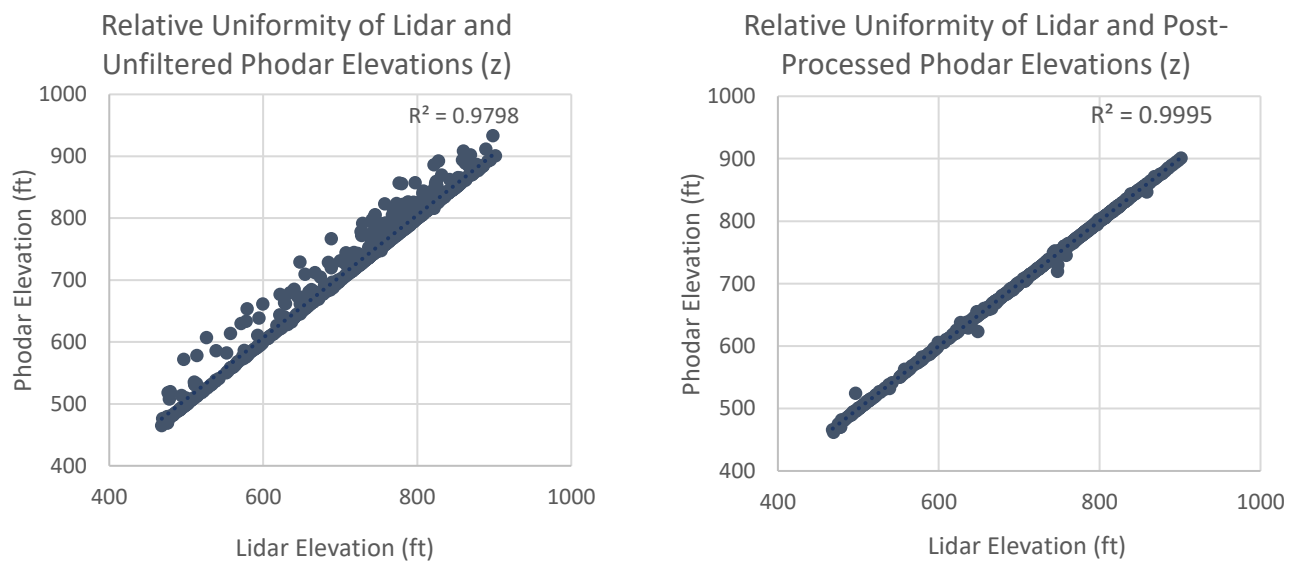


Figure 11. Comparison of the Relative Uniformity of the Phodar to the Lidar Before and After Filtering

Map Accuracy of Orthoimagery

The Root Mean Square Error (RMSE) was generated for both the phodar and lidar derived orthoimagery. The RMSE for each dataset is shown in Table 2. The RMSE, as tested for this dataset, is less than one pixel for each orthophoto dataset, which is 0.5-feet. The accuracy tested at a 95% confidence level is just over one pixel for each dataset, meaning that 95% of the positions in the phodar and lidar orthoimagery datasets should be within 0.51 feet and 0.52 feet of their true positions, respectively. The values of the six GCPs tested on each dataset can be seen in Table 3 and Table 4.

Table 2. RMSE of Lidar-based and Phodar-based Orthophotos

Lidar-Based Ortho RMSE		Phodar-Based Ortho RMSE	
RMSE easting	0.279 ft	RMSE easting	0.272 ft
RMSE northing	0.115 ft	RMSE northing	0.113 ft
RMSEr	0.302 ft	RMSEr	0.295 ft
95% Accuracy	0.523 ft	95% Accuracy	0.510 ft

Table 3. Lidar-Based Ortho GCP Test Results

Lidar-Based Ortho Ground Control Check						
Check Point	CONTROL (ft)		IMAGE (ft)		DIFFERENCE (ft)	
	EASTING	NORTHING	EASTING	NORTHING	EASTING	NORTHING
1	5194232.369	3967164.877	5194232.503	3967164.754	-0.134	0.123
2	5206675.183	3982280.662	5206675.465	3982280.534	-0.282	0.128
3	5167495.944	3960058.597	5167496.009	3960058.528	-0.065	0.069
4	5145732.671	3965334.290	5145733.000	3965334.304	-0.329	-0.014
5	5166142.594	3954497.304	5166142.500	3954497.165	0.094	0.139
6	5210982.672	3950092.866	5210983.171	3950092.714	-0.499	0.152

Table 4. Phodar-Based Ortho GCP Test Results

Phodar-Based Ortho Ground Control Check						
Check Point	CONTROL (ft)		IMAGE (ft)		DIFFERENCE (ft)	
	EASTING	NORTHING	EASTING	NORTHING	EASTING	NORTHING
1	5194232.369	3967164.877	5194232.512	3967164.812	-0.143	0.065
2	5206675.183	3982280.662	5206674.959	3982280.521	0.224	0.141
3	5167495.944	3960058.597	5167495.976	3960058.565	-0.032	0.032
4	5145732.671	3965334.290	5145733.006	3965334.241	-0.335	0.049
5	5166142.594	3954497.304	5166142.486	3954497.464	0.108	-0.160
6	5210982.672	3950092.866	5210983.171	3950092.714	-0.499	0.152

Visual Quality of Orthoimagery

A comparison of the number of DEM-derived orthophoto defects in the lidar-based and the phodar-based datasets is shown in Figure 12. Of the three defect categories tested, the phodar-based orthophotos contained fewer warped bridge defects than that of the lidar, while the lidar-based dataset contained fewer “other” warped features (buildings, retaining walls, other features) than that of the phodar. The number of smeared features was the same in both datasets. The phodar-based orthophoto dataset contained a fewer total number of DEM-derived defects than the lidar-based orthophoto dataset.

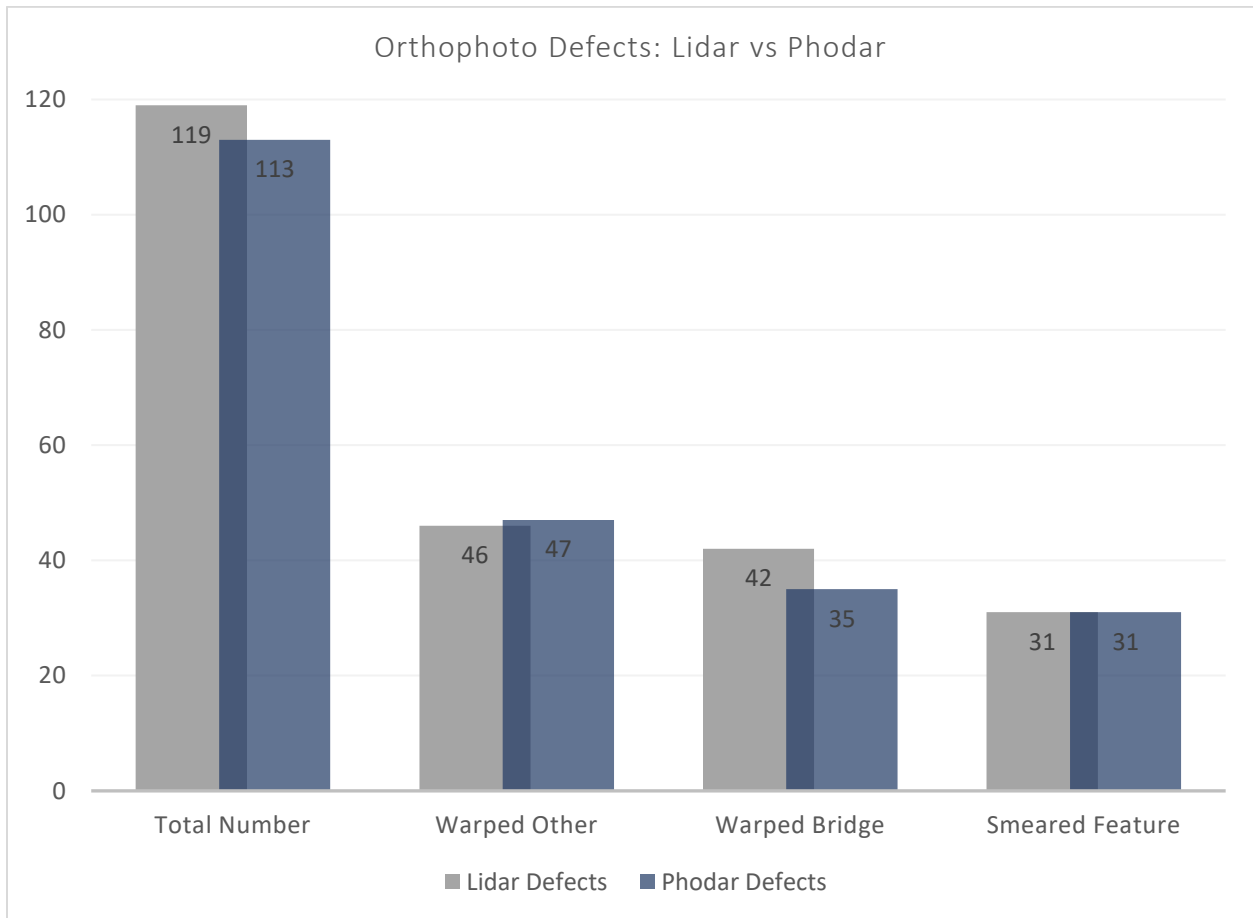


Figure 12. DEM-Derived Orthophoto Defects in Phodar and Lidar based Orthophotos

Conclusions

Conclusions for this Study

The results from this study indicate that, under certain conditions, filtered SGM phodar point clouds can be a comparable alternative to lidar for creating an orthophoto. This study focused primarily on three criteria of quality. These criteria are the uniformity of bare-earth filtered vs unfiltered SGM phodar to bare-earth lidar and the accuracy and visual quality of orthophotos that were derived from an SGM phodar point cloud. Data from a lidar point cloud were used as the reference for comparison. The conclusions of this study are discussed below.

Uniformity to Lidar

For this study, a comparison was conducted of the uniformity of elevation values of the unfiltered phodar and the phodar filtered as bare-earth to that of the lidar. As shown in Figure 5 and Figure 11, the unfiltered phodar contained points that were above ground level (high points) that were the result of vegetation, buildings, or general noise in the point cloud. Leaving these high points in the phodar point cloud significantly impacts the visual quality of the orthophoto (see Appendix 2) by creating smeared pixels. In contrast, the filtered phodar strongly agrees with the lidar dataset (see Figure 6 and Figure 11) with the lidar DEM accounting for 99.95% of the variability of the refined phodar DEM. This is further proven when the smearing in the unfiltered phodar rectification shown in Figure 11 was not present in the filtered phodar orthophoto dataset which contained the same number of smear defects as the lidar dataset, and no more. More about the orthoimagery defect findings will be discussed below in the Visual Quality section.

Visual Quality

The visual inspection of the orthoimagery datasets indicated that the phodar-derived orthophotos had five percent fewer defects than that of the lidar (see Figure 12). As such, this study concludes that an SGM phodar point cloud that is filtered to isolate bare-earth can produce orthophotos of the same or better visual quality as those produced with lidar. This conclusion is based only on testing according to the parameters outlined in this study. Additional details on this and future considerations are discussed in the Considerations for Future Studies section of this paper.

Map Accuracy

Accuracy testing in this study show that the orthophoto accuracy between the phodar-derived and lidar-derived orthoimagery was almost the same. The phodar orthophoto's RMSE was 2 percent smaller than that of the lidar which equates to 0.007 ft. While the RMSE testing that was performed used fewer than the recommended number of checkpoints than is suggested by the ASPRS, it is known that the lidar dataset used for testing meets USGS QL2 specifications and the aerotriangulation solution used for testing was performed using ASPRS guidelines for aerotriangulation. Given the known accuracy of the lidar data and the similar RMSE between the two orthophoto datasets, this suggests that the phodar ortho accuracy is similar to that of the lidar.

Summary of Conclusions

In conclusion, this study indicates that phodar can be a comparative alternative to lidar for creating accurate orthoimagery, which can result in cost-savings if a standalone lidar product is not required otherwise. While this conclusion applies to this study, it should be noted that these results are based on

a specific set of parameters which should be considered as conclusions are drawn. These considerations and recommendations for future research are also discussed below.

Considerations for Future Studies

There are considerations that should be noted for future research or improvements to this research.

The data used for this study was leaf-off imagery with a mild terrain from the Inner Bluegrass region of Kentucky. It is recommended that future testing incorporate imagery of denser vegetation and more dramatic terrain types.

It is recommended that future testing be performed on data without the inclusion of an aerotriangulation solution as input, using only the GPS and IMU for imagery orientation.

This study did not have the recommended number of ASPRS checkpoints to validate the RMSE. Future testing could incorporate the minimum number of recommended checkpoints (20) to be statistically meaningful.

In this study, small gaps in bare-earth coverage in both the lidar and phodar DEMs resulted in the need to supplement these areas with National Elevation Dataset (NED) 10 m resolution DEMs out of an abundance of caution. The void areas were so insignificant to the overall DEM that for the purposes of this study they were not evaluated. It is recommended that in future studies a comparison in the total size of data voids between similar lidar and phodar datasets be investigated.

During the image mosaicking portion of creating orthophotos, automatically generated seamlines were used to stitch together the different captures of imagery to create one seamless orthophoto. Although each of the orthophoto datasets used the exact same image takes in this study for comparison, it can be said that in areas of image overlap, other image options would have been available. This could affect the resulting number of image defects in the datasets. It is recommended that in future testing, the “best” looking images, those which have fewer defects, be chosen manually for each dataset, because a defect might be present in one image and not in another.

Acknowledgements

I would like to express appreciation to those who made this study possible. Kent Anness from Ky DGI for supporting the use of the 2019 Kentucky Statewide Orthoimagery and Lidar project data, Quantum Spatial who acquired and processed the project data for KyDGI, Ryan Griffin (of Quantum Spatial) for his expertise in filtering techniques within TerraScan, and Pat Kennelly from Penn State for advising me in this research.

Sources

- American Society for Photogrammetry and Remote Sensing. (2014). ASPRS Accuracy Standards for Digital Geospatial Data. *Photogrammetric Engineering and Remote Sensing*, Vol. 81(March 2015), A1–A26. Retrieved from http://www.asprs.org/a/society/divisions/pad/Accuracy/Draft_ASPRS_Accuracy_Standards_for_Digital_Geospatial_Data_PE&RS.pdf
- Blue Marble. (2018). LiDAR vs Photogrammetrically Generated Point Cloud Data. Retrieved from Projections: Insights from Blue Marble Geographics website: <https://blog.bluemarblegeo.com/2018/08/09/lidar-vs-photogrammetrically-generated-point-cloud-data/>
- Esri. (2019). Introduction to ortho mapping. Retrieved from ArcGIS Help website: <https://pro.arcgis.com/en/pro-app/help/data/imagery/introduction-to-ortho-mapping.htm>
- Federal Geographic Data Committee. (1999). *Content Standards for Digital Orthoimagery*. (February).
- Federal Geographical Data Committee. (1998). Geospatial Positioning Accuracy Standards Part 3 : National Standard for Spatial Data Accuracy. *National Spatial Data Infrastructure*, 28. Retrieved from <http://www.fgdc.gov/standards/projects/FGDC-standards-projects/accuracy/part3/chapter3>
- Gehrke, S., Morin, K., Downey, M., Bohrer, N., & Fuchs, T. (2010). Semi-global matching: an alternative to lidar for dsm generation? *International Archives of the Photogrammetry, Remote Sensing and Spatial Information Sciences*, XXXVIII-B1, 1–6.
- Gehrke, S., Uebbing, R., Downey, M., & Morin, K. (2011). Creating and using very high density point clouds derived from ADS imagery. *American Society for Photogrammetry and Remote Sensing Annual Conference 2011*, 156–165. Retrieved from http://www.asprs.org/a/publications/proceedings/Milwaukee2011/files/Gehrke_1.pdf
- Hirschmüller, H. (2008). Stereo processing by semiglobal matching and mutual information. *IEEE Transactions on Pattern Analysis and Machine Intelligence*, 30(2), 328–341. <https://doi.org/10.1109/TPAMI.2007.1166>
- Hohle, J. (1996). Experiences with the production of digital orthophotos. *Photogrammetric Engineering and Remote Sensing*, 62(10), 1189–1194.
- Kentucky Division of Geographic Information. (2019). KYAPED 2019 Project Area - 6 Inch Imagery. Retrieved from <https://kygeoportal.ky.gov/geoportal/catalog/search/resource/details.page?uuid=%7B370E29E4-5B19-4D4A-860E-8D864346D431%7D>
- KYAPED. (2019a). *6-Inch Orthoimagery produced by Quantum Spatial, Inc*. Retrieved from <ftp://ftp.kymartian.ky.gov/kyaped>
- KYAPED. (2019b). *Ground Control Points 2012 - 2019*. Retrieved from <ftp://ftp.kymartian.ky.gov/kyaped/GroundControlPoints>
- KYAPED. (2019c). *QL2 Lidar produced by Quantum Spatial, Inc*. Retrieved from <ftp://ftp.kymartian.ky.gov/kyaped/LAZ>
- Osińska-Skotak, K., Bakuła, K., Jełowicki, Ł., & Podkowa, A. (2019). Using Canopy Height Model Obtained

with Dense Image Matching of Archival Photogrammetric Datasets in Area Analysis of Secondary Succession. *Remote Sensing*, 11(18), 2182. <https://doi.org/10.3390/rs11182182>

Quantum Spatial. (2019a). *2019 Kentucky Statewide LiDAR Project for KyDGI*.

Quantum Spatial. (2019b). *2019 Kentucky Statewide Orthoimagery Project for KyDGI*. Lexington, KY.

Švec, Z., & Pavelka, K. (2016). Preparation of the digital elevation model for orthophoto CR production. *International Archives of the Photogrammetry, Remote Sensing and Spatial Information Sciences - ISPRS Archives*, 41(July), 107–113. <https://doi.org/10.5194/isprsarchives-XLI-B3-107-2016>

Trimble. (2020). *Inpho 10*. Trimble.

United States Geological Survey. (2019). *Lidar Base Specification version 2.1*. Retrieved from <https://www.usgs.gov/core-science-systems/ngp/ss/lidar-base-specification-v-21-table-contents>

University of Kentucky. (2020). Franklin County Kentucky Topography. Retrieved from <https://kgs.uky.edu/kgsweb/download/gwatlas/gwcounty/franklin/frankline1.jpg>

USGS. (2020). USGS 3D Elevation Program. Retrieved from <https://www.usgs.gov/core-science-systems/ngp/3dep/3dep-data-acquisition-status-maps%0A>

Widyaningrum, E., & Gorte, B. G. H. (2017). Comprehensive comparison of two image-based point clouds from aerial photos with airborne LiDAR for large-scale mapping. *International Archives of the Photogrammetry, Remote Sensing and Spatial Information Sciences - ISPRS Archives*, 42(2W7), 557–565. <https://doi.org/10.5194/isprs-archives-XLII-2-W7-557-2017>

Appendix



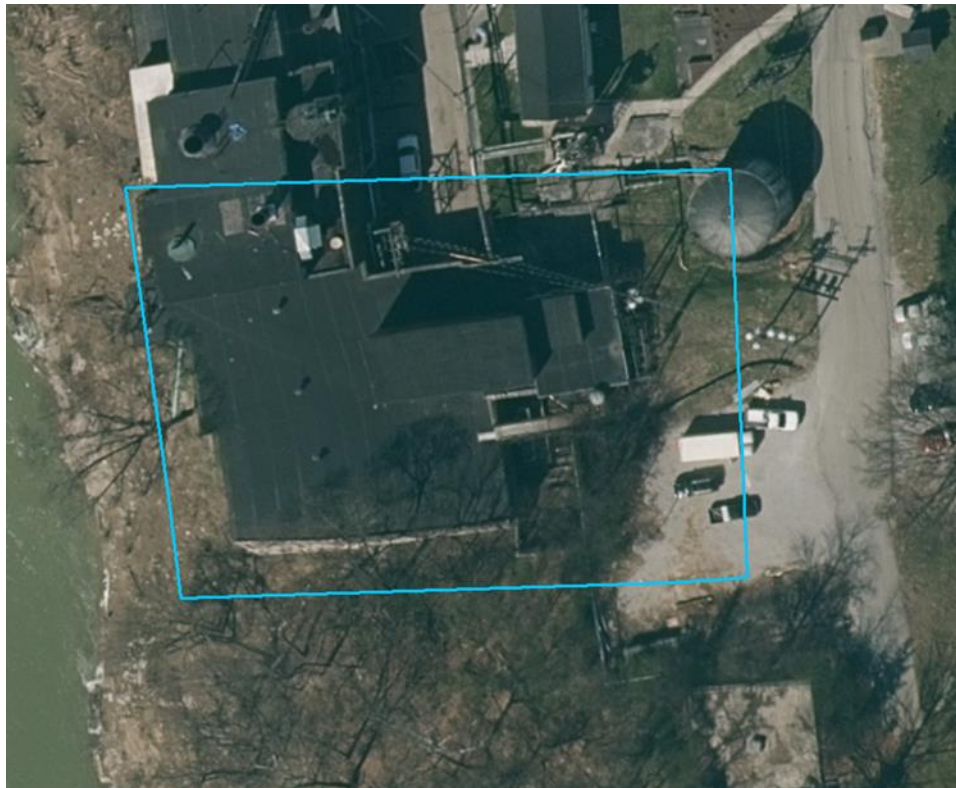
Appendix 1. Example of Smeared Orthoimagery Pixels



Appendix 2. Example of Smearing and Warping in Orthoimagery Pixels Encountered During Testing with Unfiltered Phodar



Appendix 3. Example of Bridge Warping in Orthoimagery



Appendix 4. Example of Building Warping